Including Temperature Effects in the F15 RADCAL Correction

Kyle Hilburn
Remote Sensing Systems
http://www.remss.com

1. Introduction

On 14 August 2006, the radar calibration (RADCAL) suite was activated on DMSP F15. The RADCAL suite consists of a pair of 150 MHz and 400 MHz beacons. On orbit testing conducted in August 2005 confirmed that transmissions from the 150 MHz RADCAL beacon produced strong interference in the SSM/I 22 GHz vertical polarization (22V) channel. No effect was apparent in the 19 or 37 GHz channels, and a small effect was found for the 85 GHz horizontal polarization channel.

Previously, we developed a simple correction to mitigate the impact of the RADCAL beacon contamination on the F15 SSM/I ocean retrievals (Hilburn and Wentz, 2008; hereafter referred to as HW08). We developed a simple linear-regression to predict the 22V brightness temperature based on the 19 and 37 GHz horizontal and vertical polarization brightness temperatures. The regression was derived using data from 2005 (i.e., before the beacon was turned on). The relationship fits with a standard deviation of 2.33 K, and it fits well over the whole range of ocean brightness temperatures. The RADCAL effect was isolated by finding the difference between the measured and the predicted 22V brightness temperature using data from 2007 (i.e., after the beacon was turned on). This technique found a bias of 10 K with an 8 K dependence on along-scan cell position. This technique led to a static table of brightness temperature offsets (Fig. 1), with one value for each of the 64 along-scan cells. These values are available online at http://www.remss.com/ssmi/support/f15_radcal_table_22v.txt.

In the beginning of 2008, just as HW08 was published, time series of brightness temperature differences showed a slight oscillation (Fig. 2 in HW08). It was difficult to determine exactly what was happening with the small amount of data, but this was the first evidence that the RADCAL interference also depended on the temperature of the satellite electronics.

In early 2009, the nature of the temperature dependent RADCAL effects became clear during a very strong cold event. As F15 drifts earlier in the day (Fig. 2), its thermal environment experiences cold periods resulting from F15 being eclipsed by earth's shadow. Figure 3 shows retrieval behavior during the two minor cool events in 2008 and the strong cold event in early 2009. The signature of RADCAL interference can be seen: rain and wind retrievals are biased low, while cloud and vapor retrievals are biased high. The biases in 2008 are on the order of 10%, but in 2009, the biases become larger than 40%. These are on the same order as the biases before any RADCAL correction was applied. Figure 4 shows the brightness temperature differences along with the hot load temperature, which is used here as a proxy for the temperature of the satellite electronics. It is clear that the biases are related to the hot load temperature, and Fig. 4 suggests the relationship is not linear.

The purpose of this technical report is to document our new RADCAL correction that includes a dependence on hot load temperature. This correction is an improvement on HW08. The new correction removes most of the brightness temperature bias while reducing the standard deviation by half (Fig. 4). Note that the correction does not completely reduce the standard deviation to the original levels. The new correction is capable of reducing retrieval biases to 10% during the coldest events (Fig. 3). That is, while we can "put a lid" on the RADCAL interference effects and produce data that are useful for meteorological analysis, F15 data after August 2006 should not be used for climate studies.

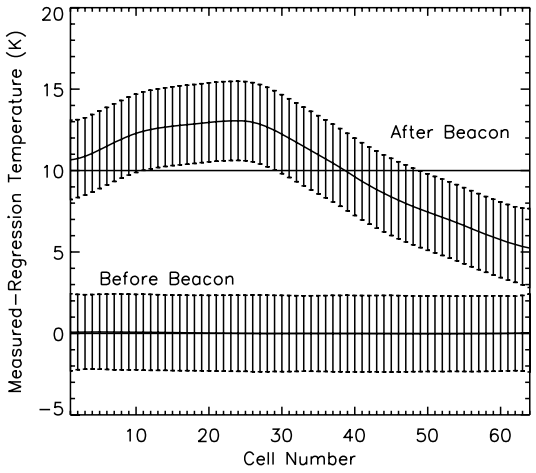

Figure 1. Cell-average difference between the measured and predicted 22V brightness temperature before the beacon was turned on (year 2005) and after (year 2007). These averages are for the rain-free ocean equatorward of 60 degrees latitude for the 64 SSM/I footprints along the scan. The "after" curve is the HW08 correction.

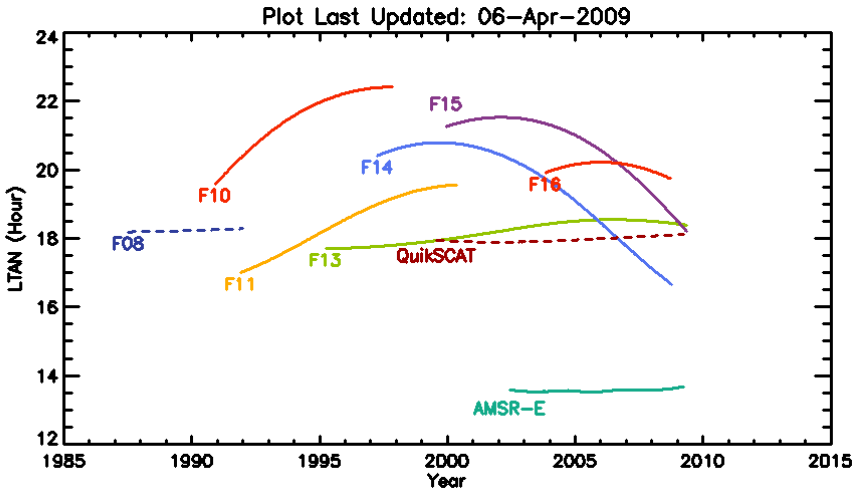

Figure 2. Time series of local equatorial crossing time. Dashed curves indicate that descending time is plotted. F15 is the purple curve.

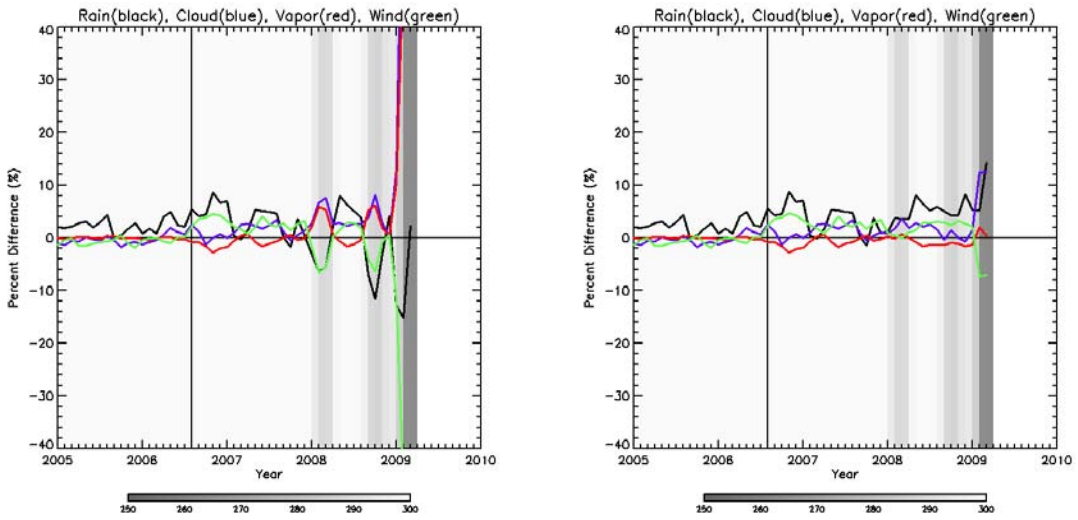

Figure 3. Time series of the difference between F15 and F13 retrievals using the HW08 RADCAL correction (left) and using the new temperature-dependent RADCAL correction in this report (right). The hot load temperature is shown in shades of grey with the color scale at the bottom of the plot. The start of beacon operation is marked with a black vertical line in August 2006. Notice that 2008 has two cool events, one in the spring and one in the fall. The very cold event at the beginning of 2009 has temperatures about 50 K less than the nominal values. The RADCAL signature of low wind (green) and rain (black) retrievals and of high vapor (red) and cloud (blue) retrievals can easily be seen during the cold events. The new temperature dependent correction reduces the RADCAL effects.

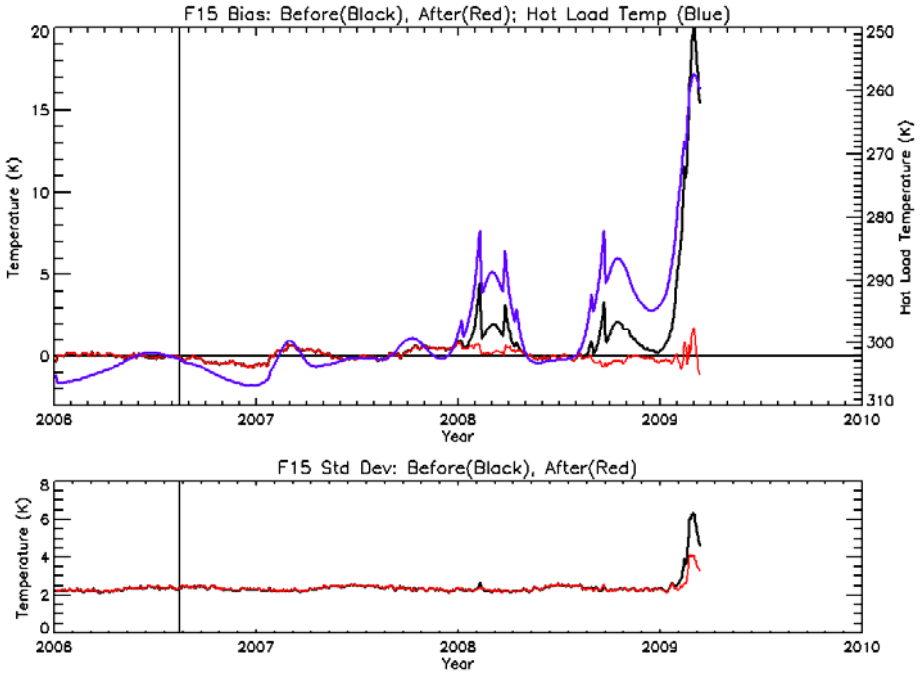

Figure 4. Time series of the measured minus predicted 22V brightness temperature bias (top) and standard deviation (bottom). Shown are: data corrected with HW08 (black line), data corrected with the temperature dependent correction in this report (red line), and the hot load temperature (blue line, which corresponds to the right axis). Note: the right axis for hot load temperature is reversed.

2. Model for Temperature-Dependent RADCAL Interference

Maps of F15's hot load temperature (Fig. 5) show that it varies with latitude and has small day/night differences. Figure 5 does not show that hot load temperature also has a seasonal cycle with an amplitude and phase that change over time as the satellite's orbit drifts. The examples in Fig. 5 show how the hot load temperature changes from "normal" conditions in February 2007, to cool conditions in February 2008, and to cold conditions in February 2009. These conditions do not last all year long, but occur roughly in the spring and fall (Fig. 4) when F15 is eclipsed by earth's shadow.

There are two basic models that could be adapted to include the hot load temperature dependence: additive and multiplicative. The additive model is the simplest model and we tried it first; however we will show that it does not fit the data well. The multiplicative model is the next simplest, and we found it does fit the data well. The form of the HW08 correction with no temperature dependence is

$$T_{corr} = T - r[cell] \quad (1)$$

where T_{corr} is the corrected brightness temperature, T is the uncorrected brightness temperature, and $r[cell]$ is the table of values for each of the 64 along scan cell positions shown in Fig. 1. The additive model has the form:

$$T_{corr} = T - r[cell] - t[T_{HL}] \quad (2)$$

where $t[T_{HL}]$ is either an explicit function of hot load temperature, T_{HL}, or a table of values like r. The advantage of using a function, rather than a table, is that T_{HL} may assume new larger or smaller values in the future not observed before. This is not a problem with r, since *cell* will always be in the range [1,64] for the 19, 22, and 37 GHz channels. The hazard with using a function, of course, is that we might extrapolate our regression in ways that could be inappropriate. Note that t has units of temperature, like r. The other possibility is the multiplicative model, which has the form:

$$T_{corr} = T - r[cell] \bullet s[T_{HL}] \quad (3)$$

where $s[T_{HL}]$ is a non-dimensional quantity that modulates r. Figure 6 compares the additive and multiplicative models. In both cases, a similar dependence on hot load temperature is used, and is described in the next paragraph. The additive model (Fig 6B) has a shape in *cell* that does not match the data (Fig. 6A) as well as the multiplicative model does (Fig. 6E). This is clearly shown by the differences between the models and the data (compare the additive model, Fig. 6C, with the multiplicative model, Fig. 6F).

The RADCAL interference is not a linear function of hot load temperature. Figure 7 shows that a quadratic function of temperature captures the dependence very well. The correction we use is

$$s[T_{HL}] = 8.51691\text{E-}4 \bullet T_{HL}^{\,2} - 5.18557\text{E-}1 \bullet T_{HL} + 7.98977\text{E+}1 \quad (4)$$

The best retrieval results are obtained when s for T_{HL} larger than 298 K are kept to a value of 1. We have restricted the allowable range of hot load temperature to get no lower than 250 K. This caps the maximum value of s near 3.5. It is possible that we will observe colder temperatures that might require larger adjustments. If this happens, we will have more data and can reformulate s with the new information. We have also tried using higher order polynomials for s and special types of weighting in regressing for s. We have even used a pure table-based approach:

$$T_{corr} = T - q[cell, T_{HL}] \quad (5)$$

where q is a table of values with the dimensions *cell* and T_{HL}. We did this to test whether the deviations from our simple fit (the difference between the black and red lines in Fig. 7) would make a measurable impact on the retrievals. None of these more complicated attempts yielded improvements, in fact, these actually made some of the retrievals worse. Remember that at this stage, we are working in terms of the difference between predicted and measured 22V brightness temperature. We have not made an attempt to "optimize" our correction in terms of the differences of the retrievals from some standard of truth (say F13 or NWP output). That sort of approach would require a more complicated methodology.

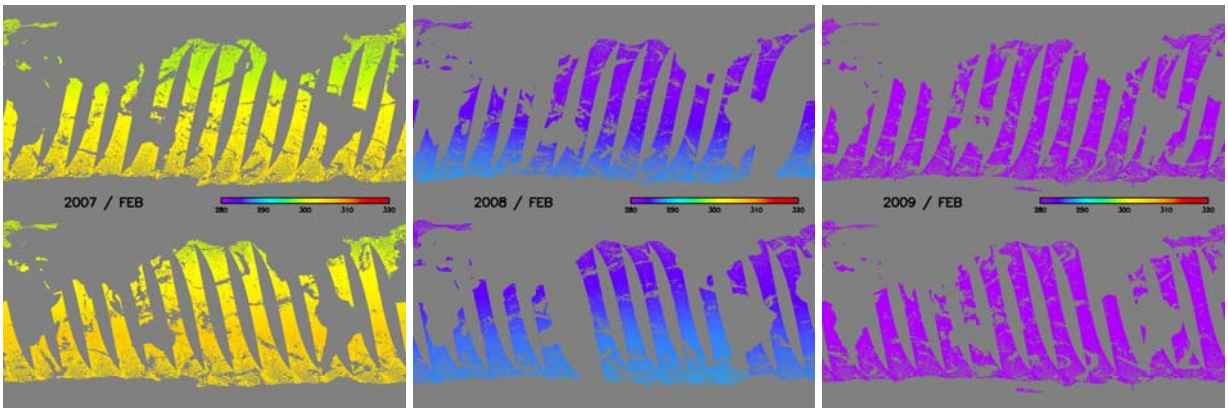

Figure 5. Maps of hot load temperature for morning (top) and evening (bottom) passes from the first day of February 2007 (left), 2008 (middle), and 2009 (right).

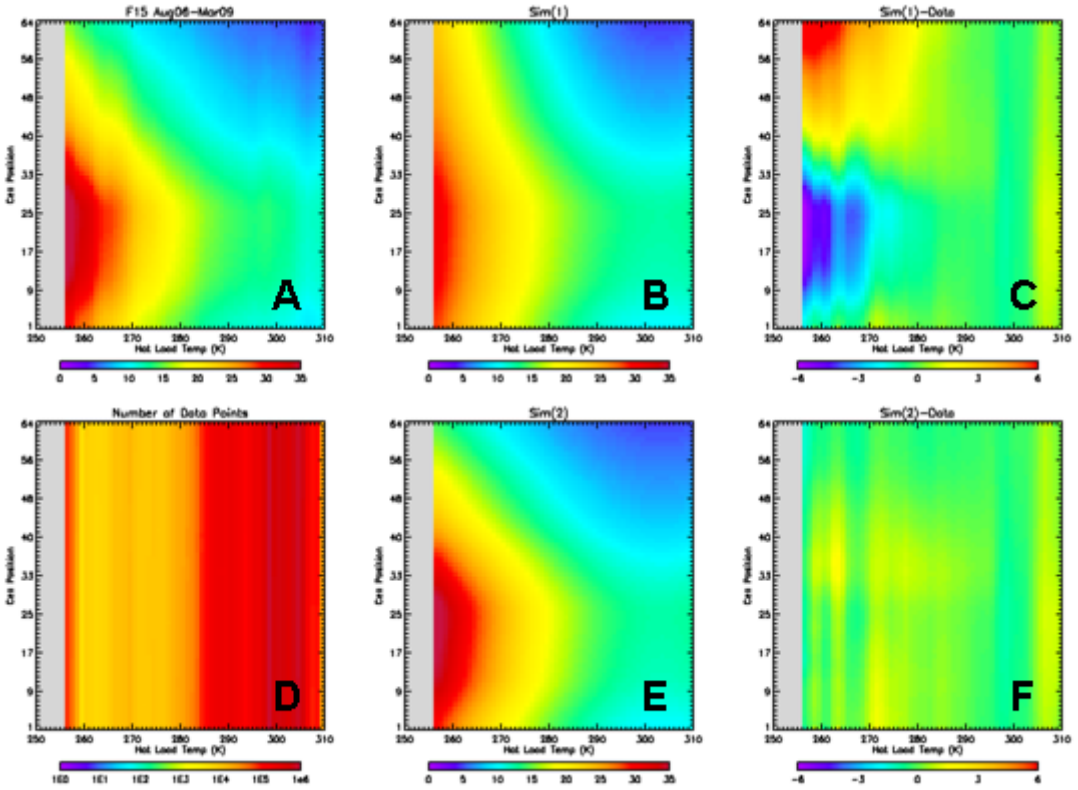

Figure 6. Comparison of the additive and multiplicative models for RADCAL interference. All panels display their information relative to hot load temperature (horizontal axis) and cell (vertical axis) using the color scale shown underneath the panel. (A) The measured – predicted 22V brightness temperature difference given by the F15 data. (B) Difference predicted by the additive model. (C) Difference between the additive model and the data (panel C is panel B minus panel A). (D) Number of observations in each hot load temperature and cell bin. (E) 22V brightness temperature difference predicted by the multiplicative model. (F) Difference between the multiplicative model and the data (panel F is panel E minus panel A). It can be seen that the multiplicative model fits the data better because panel F contains mostly green color compared to panel C.

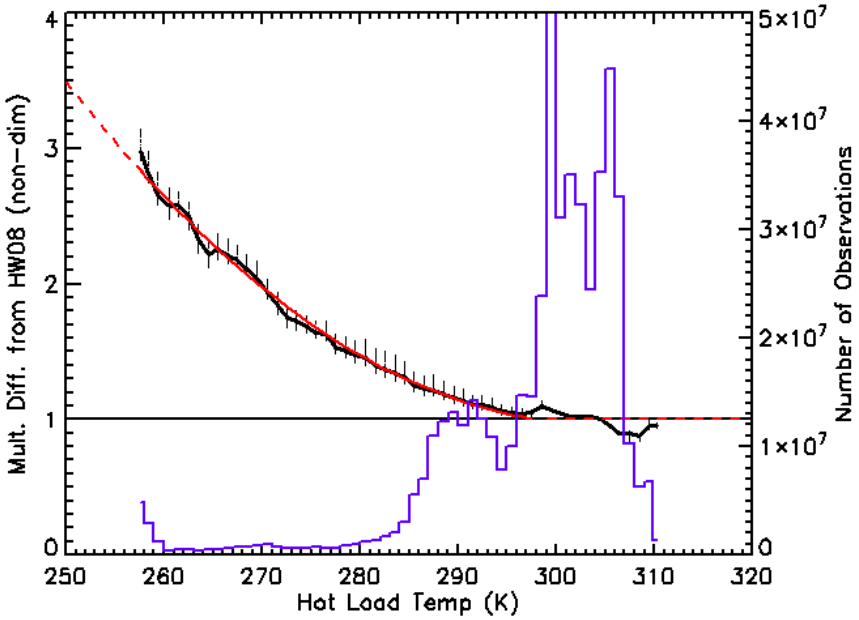

Figure 7. The multiplicative difference from the HW08 tabular values as a function of hot load temperature (black line) with the variability (from different cell positions) shown by the small vertical lines. Also shown are a quadratic regression in hot load temperature (red) and the number of observations in each hot load temperature bin (blue line, corresponds to axis on right side). Note that the red line is $s[T_{HL}]$. The best results were obtained with a value of 1 for temperatures greater than 298 K (shown by a dashed red line). Data were available for temperatures as low as 257 K. The extrapolation to lower temperatures (red dashed line) is allowed down to 250 K. This quadratic behavior with temperature is the same for the additive model as well.

3. Results

We have examined differences between F15 retrievals and retrievals from other SSM/I satellites close in time (F14 in HW08 and F13 in this report) both before and after making the correction. The standard analyses we have performed includes: global monthly average time series, zonal average differences (and how they change over time), joint-PDFs, and time-average difference maps. We also routinely examine raw daily gridded retrievals and compare different storms and meteorological features from different satellites. The time-average maps are helpful for interpreting zonal averages, and the joint-PDFs are helpful for showing the systematic biases and increases in variance in the retrievals. Global monthly average time series have already been shown (Fig. 3). In this section, we will show zonal averages because they are a very concise metric, summarizing most of the information in a small amount of space on the page. We will also show one storm example.

Figure 8 shows zonal average differences between F15 (after applying the temperature dependent correction in this report) versus F13. Rain rate retrievals, which are a very sensitive retrieval, have biases larger than 10% over large areas. The statistical inhomogeneity of rain also contributes to the noisiness of the curves. Water vapor and wind speed retrievals have the smallest biases – nowhere larger than 10% for wind and nowhere larger than 5% for vapor.

Differences as a function of latitude are fairly flat, except for rain. The purple, blue, and green curves for wind and vapor are concentrated near the zero line – showing the sudden decrease in quality when the RADCAL period begins (orange and red curves). The rainbow progression from purple to red for the cloud and rain curves indicate that F15 has spurious trends relative to F13 that have been greatly exacerbated by RADCAL interference. Figure 8 also separates day and night passes, and while we find different patterns that change differently over time, there is not a substantial difference between the magnitudes of the patterns. That is to say, differences are not confined to day or night, but are present for both.

Fig. 9 shows one example of a storm off the east coast of the United States. The corrected F15 retrievals are much closer to the F13 retrievals than the uncorrected retrievals, but are not without some issues. In particular, it appears that the water vapor for the corrected retrievals have a larger rain contamination signal than F13. This example also illustrates that in addition to the biasing of the uncorrected retrievals, the RADCAL interference also has the effect of increasing the area of rain flagged wind speeds and it extends the ice mask over larger areas in unrealistic ways.

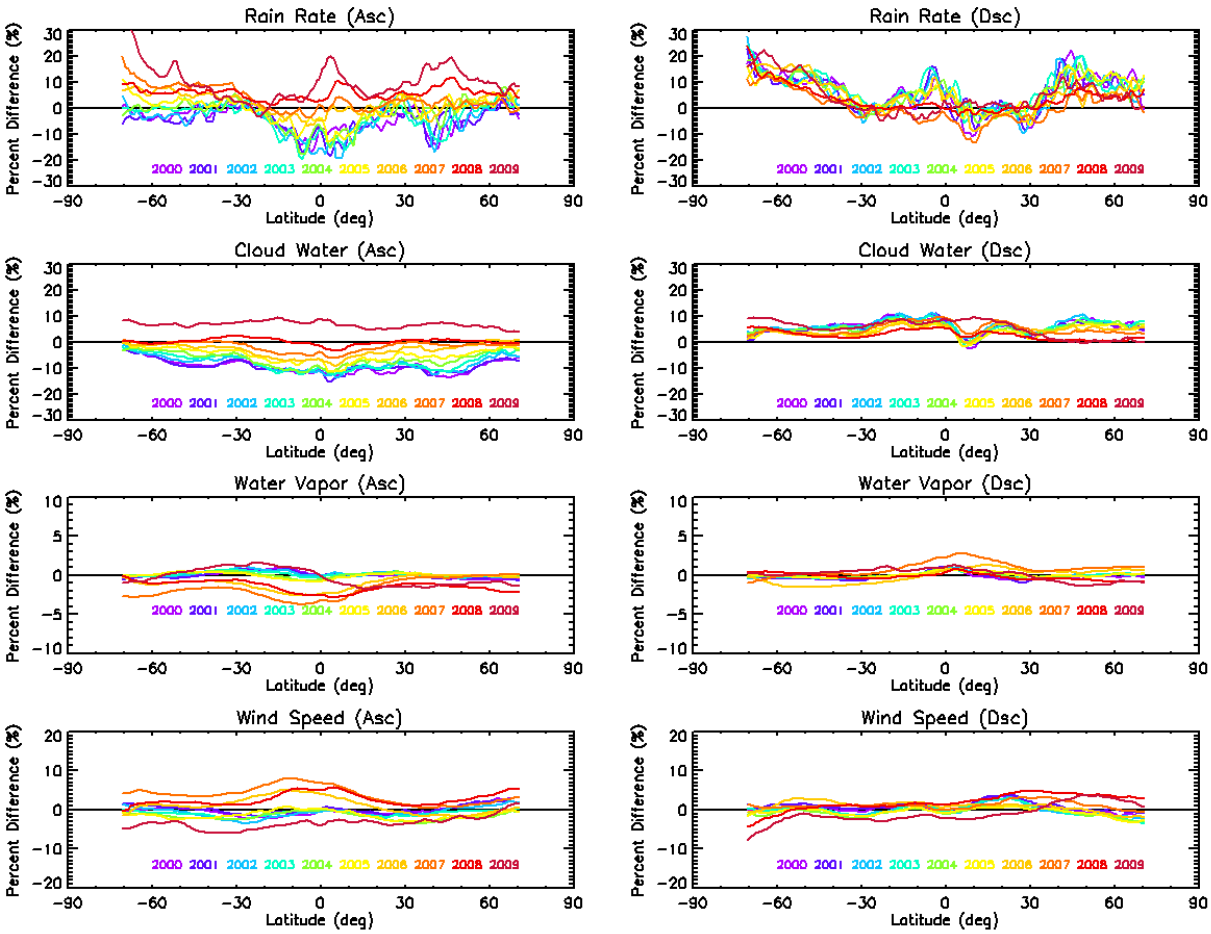

Figure 8. Zonal average F15-F13 differences for the years 2000 through 2009 (each year a different color) for rain rate (top panels), cloud water (second from the top), water vapor (second from the bottom), and wind speed (bottom panels) separating the ascending swaths (panels in left column) and descending swaths (panels in right column). These are the differences after applying the temperature dependent RADCAL correction described in this report. The differences are expressed in units of percent by dividing each F15-F13 yearly curve by the global average F13 value for that year. This makes the relative differences between the retrievals more clear, while preserving the relevant latitudinal behavior. Note that the different parameters have different scales on the vertical axis.

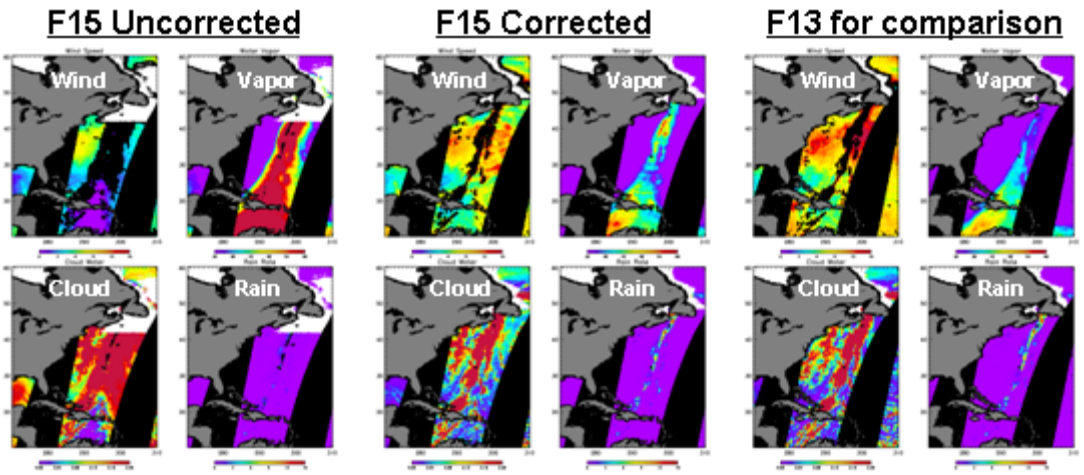

Figure 9. A storm example off the U.S. east coast (3 March 2009). The figure consists of three clusters of figures: F15 uncorrected (left), F15 corrected (middle), and F13 for comparison (right). Each cluster has four panels that give wind speed (top, left), water vapor (top, right), cloud water (bottom, left), and rain rate (bottom, right). Note that the RADCAL interference not only biases the uncorrected retrievals, but also causes increased rain flagging of wind speeds and extends the ice mask over larger areas. The color scales are: wind (0-15 m/s), vapor (30-60 m/s), cloud (0-0.2 mm), and rain (0-15 mm/hr).

Acknowledgements

This work has been supported under NASA contract NNG07HW15C, Precipitation Measurement Mission (PMM).

References

Hilburn, K. A. and F. J. Wentz, 2008: Mitigating the impact of RADCAL beacon contamination on F15 SSM/I ocean retrievals, *Geophys. Res. Lett.*, **35**, L18806, doi:10.1029/2008GL034914.